Self-consistent theory of superconducting mesoscopic weak links

A. Levy Yeyati, A. Martín-Rodero, and F. J. García-Vidal
Departamento de Física de la Materia Condensada C-XII,
Facultad de Ciencias, Universidad Autónoma de Madrid, E-28049 Madrid, Spain
(Received 20 July 1994)

A microscopic model for describing a superconducting mesoscopic weak link is presented. We consider a model geometry consisting of a narrow channel coupled to wider superconducting electrodes which act as reservoirs fixing the asymptotic values of the complex order parameter. For this model, the Bogoliubov–de Gennes equations are discretized and solved self-consistently using a nonequilibrium Green-function formalism. The transport properties and the electronic excitation spectra of this system are studied for the different regimes that can be reached by varying parameters like coherence length, constriction length, normal transmission coefficient and temperature. We study in detail the transition from the point-contact limit to the infinite channel length case, analyzing the maximum Josephson current that can be sustained by the weak link as a function of its transmission coefficient and length. It is also shown that for a constriction size ranging from zero to several times the coherence length, most of the current is carried, inside the constriction region, by bound states within the superconducting energy gap. These states correspond to Cooper pairs with binding energies smaller than the superconducting gap and which are spatially extended along the channel region, decaying exponentially inside the reservoirs. The importance of the self-consistent determination of the order parameter along the weak link is illustrated by analyzing different profiles obtained for channel lengths of the order of the coherence length. For temperatures not very close to T_c, our microscopic calculation predicts the appearance of features which cannot be obtained from Ginzburg-Landau theory.

I. INTRODUCTION

The interest in the physics of submicrometer superconducting devices[1] stems to a great extent from the special combination, taking place in this kind of system, of normal electron phase coherence in the nanometer scale together with quantum macroscopic effects associated with the superconducting state.

Some of the superconducting mesoscopic devices which are recently receiving more attention include normal-metal–superconductor (NS) junctions and superconductor-semiconductor (Sm) junctions where Andreev reflection processes play a crucial role,[2–5] and superconducting mesoscopic point contacts which can exhibit quantization of the Josephson current.[6]

A theoretical description of the transport properties in all these submicrometer devices has to deal with spatial inhomogeneities due to the presence of geometrical boundaries and interfaces between different materials; in a superconducting mesoscopic device this could lead to strong spatial variations of the superconducting order parameter.

In normal mesoscopic devices the problem of computing their transport properties has been historically addressed by different approaches. One is based on the scattering picture proposed by Landauer[7] and generalized to more complicated situations (multichannel and multilead cases) by different authors.[8] Another approach, especially suited to deal with local inhomogeneities, relies on the use of a localized representation for the electronic states of the sample, whose transport properties can then be efficiently calculated in terms of Green functions.[9]

The scattering approach has been extended to superconductors by Blonder *et al.*[10] and more recently applied to a mesoscopic NS junction by Beenakker,[2] who has obtained a multichannel generalization of the result of Blonder *et al.*, and to different superconducting devices by other authors.[3–5] Despite its many advantages, the scattering approach is probably not the most convenient starting point for a self-consistent determination of the order parameter in situations where its spatial variations on a scale smaller or comparable to the superconducting coherence length (ξ_0) may be important. For instance, this can be the case in a NS junction when there is an appreciable induction of superconductivity in the normal electrode by a proximity effect.[11] Another example is that of a superconducting weak link with a length comparable to ξ_0, in which case, as shown in the present paper, the self-consistent determination of the order-parameter profile becomes unavoidable.

In a recent letter,[12] we have presented a theoretical approach based on a local description of the superconducting mesoscopic system, in which a nonequilibrium Green-function formalism is used. This method provides an efficient way of calculating the transport properties and the spatial variations of the self-consistent order parameter through the whole system. The aim of the present paper is to discuss in further detail our approach, taking

as a test system a mesoscopic superconducting weak link (SWL) at zero voltage. We shall consider a model geometry in which two wide superconducting electrodes are coupled by a narrow channel. As discussed by Likharev[13] in his review on weak links, there are two main reasons for the basic interest on this kind of systems: First, weak links of reduced dimensions exhibit the Josephson effect in nontunnel conditions and are especially suitable for a variety of applications. On the other hand, for weak links of increasing length (larger separation between electrodes), the transition from the Josephson effect to bulk transport in superconductors can be studied. This last question is addressed in detail in the present paper.

Traditionally, the transport properties of SWL's have been analyzed with the help of phenomenological Ginzburg-Landau (GL) theory.[14] However, GL theory is only valid for a limited temperature range ($T \to T_c$) and, furthermore, the implicit hypothesis of slow spatial variation of the order parameter in GL theory, as derived from the microscopic theory,[15] breaks down for a general mesoscopic geometry. In these situations a complete self-consistent solution of the Bogoliubov–de Gennes equations would be necessary.[16] As we show in this work, features in the order parameter profile associated with length scales smaller than ξ_0, like the Fermi wavelength and some geometrical length scales, emerge in a natural way from the microscopic calculation. In addition, another result arising from the microscopic calculation, which could never be obtained from GL theory, is the existence of bound states inside the superconducting gap playing a fundamental role in the transport through the weak link.

The plan of the present paper is the following: In Sec. II we introduce our discretized (tight-binding) model for a general constriction geometry, and discuss the conditions for the fulfillment of current conservation within our model. In Sec. III the nonequilibrium Green-function formalism in a superconducting broken-symmetry representation is presented, giving the expression for the relevant quantities within this formalism and details about its self-consistent determination. Section IV is devoted to an analysis of the transition from the point-contact regime to infinite one-dimensional (1D)-superconductivity, discussing the maximum current that can flow as a function of the weak-link transmission coefficient. The analysis of the spectral densities reveals the presence of a slowly increasing number of bound states inside the superconducting gap. It is shown that these states give the main contribution to the supercurrent in the constriction region and decay exponentially inside the 3D electrodes.

In Sec. V the importance of the self-consistent determination of the order parameter is illustrated by discussing the different type of profiles that can be obtained for a mesoscopic SWL. We emphasize those features that cannot appear in a GL calculation. Finally, in Sec. VI the effects of temperature both in the current-phase relationship and self-consistent profiles are analyzed. We find that, except very near T_c, there is no simple scaling of the system properties with temperature.

The paper is closed with some concluding remarks.

II. DISCRETIZED MODEL FOR A MESOSCOPIC WEAK LINK

We consider a model weak link like the one depicted in Fig. 1. The constriction width W is assumed to be smaller than the penetration length and comparable to the Fermi wavelength λ_F, leading to a small number of conducting channels. The constriction length L_c can be varied from the point-contact regime $L_c/\xi_0 \to 0$ to the opposite case $L_c/\xi_0 \to \infty$, recovering in this case the limit of a homogeneous quasi-1D superconductor. Phase coherence is assumed to be preserved along the whole system.

The wider regions representing the left and right electrodes ensure the asymptotic convergence of the complex order parameter Δ to its bulk value. This model geometry would be similar to the one-dimensional structure with electrodes in equilibrium model proposed by Likharev.[13]

Our aim will be the complete self-consistent solution of the microscopic Bogoliubov–de Gennes equations[17] for this system. For this purpose we find it convenient to formulate these equations using a site representation for the electronic states. This representation can be viewed either as a tight-binding description of the electronic states or as a discretization of the Bogoliubov–de Gennes equations (a simple scaling of the parameters would account for the use of one or another description). For the electron-electron interaction we make the usual simplifying assumption of taking it as a contact attractive interaction,[17] which in a site representation adopts the form of a negative-U Hubbard-like local term.

Within these assumptions, the mean-field model Hamiltonian giving rise to the Bogoliubov–de Gennes equations for our system can be written as[12]

$$\hat{H} = \sum_{i,\sigma} (\epsilon_i - \mu) c^\dagger_{i\sigma} c_{i\sigma} + \sum_{i \neq j,\sigma} t_{ij} c^\dagger_{i\sigma} c_{j\sigma} + \sum_i (\Delta^*_i c^\dagger_{i\downarrow} c^\dagger_{i\uparrow} + \Delta_i c_{i\uparrow} c_{i\downarrow}), \quad (1)$$

where, for the zero voltage case, the chemical potential μ is a constant throughout the whole system and the sum over i and j in the second term is restricted to nearest neighbors only. The self-consistent conditions for the or-

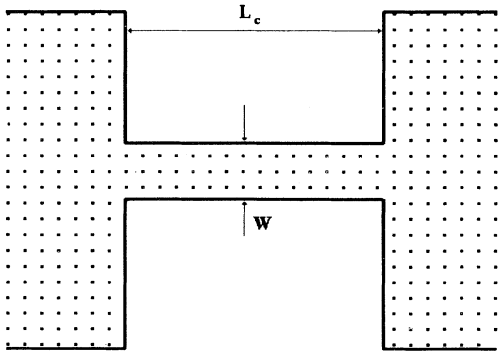

FIG. 1. Schematic representation of our discretized model weak link.

der parameter on each site are given by

$$\Delta_i = -U_i \langle c_{i\downarrow}^\dagger c_{i\uparrow}^\dagger \rangle, \tag{2}$$

where U_i is the attractive $e-e$ interaction at site i. By choosing appropriately the U_i, t_{ij}, and ϵ_i in the three regions (left electrode, constriction, right electrode) one can model different situations: S-S'-S, S-N-S, S-Sm-S, etc. In this paper we shall concentrate in the first situation, assuming the same *bulk* value of the order-parameter modulus $|\Delta|$ on the three separate regions and fixing the value $\epsilon_i = \mu = 0$ (which implies $e-h$ symmetry) in the whole system for simplicity. This criterion fixes the ratio U_i/t_{ij} inside the three regions. The total phase drop along the whole system $\phi = \phi_L - \phi_R$ is imposed as a boundary condition, ϕ_L and ϕ_R being the the bulk value of the order-parameter phase on the left and right electrodes, respectively. A relevant parameter is the superconducting coherence length in the constriction $\xi_0(T)$, which in our model can be estimated as $\xi_0(T) = 2t_c/\pi\Delta(T)$, where t_c is the hopping parameter in this region.

The current between two neighboring sites ij is given by

$$I_{ij}(t) = \frac{ie}{\hbar} \sum_\sigma \left[t_{ij} \langle c_{i\sigma}^\dagger(t) c_{j\sigma}(t) \rangle - t_{ji} \langle c_{j\sigma}^\dagger(t) c_{i\sigma}(t) \rangle \right]. \tag{3}$$

In the zero-voltage case the supercurrent does not depend explicitly on time. It is worth noticing that current conservation is only fulfilled when the solution of the mean-field superconducting Hamiltonian is fully self-consistent.[10,12,18,19] Indeed, current conservation provides a stringent test of self-consistency.

The proof of this statement is straightforward when using a site representation. Starting from the equation of motion for the charge density operator at site i ($\hat{\rho}_i = -e \sum_\sigma c_{i\sigma}^\dagger c_{i\sigma}$) we find

$$\begin{aligned} \frac{\partial \langle \hat{\rho}_i \rangle}{\partial t} &= \frac{i}{\hbar} \langle [\hat{\rho}_i, \hat{H}] \rangle \\ &= -\sum_j I_{ij} + \frac{2ie}{\hbar} \left(\Delta_i \langle c_{i\uparrow} c_{i\downarrow} \rangle - \Delta_i^* \langle c_{i\downarrow}^\dagger c_{i\uparrow}^\dagger \rangle \right). \end{aligned} \tag{4}$$

The last term appears due to the fact that $\hat{H}$ does not conserve the particle number. However, when the self-consistency condition [Eq. (2)] is fulfilled, this term vanishes, and the continuity equation $\frac{\partial \langle \hat{\rho}_i \rangle}{\partial t} + \sum_j I_{ij} = 0$ is recovered for every site.

III. SOLUTION IN TERMS OF NONEQUILIBRIUM GREEN FUNCTIONS

The averaged quantities appearing in Eqs. (2) and (3) can be expressed in terms of nonequilibrium Green functions.[20] For the description of the superconducting state it is useful to introduce spinor field operators,[21] which in a site representation are defined as

$$\hat{\psi}_i = \begin{pmatrix} c_{i\uparrow} \\ c_{i\downarrow}^\dagger \end{pmatrix}, \quad \hat{\psi}_i^\dagger = \begin{pmatrix} c_{i\uparrow}^\dagger & c_{i\downarrow} \end{pmatrix}. \tag{5}$$

Then, the different correlation functions appearing in the Keldysh formalism adopt the standard causal form

$$\hat{G}_{ij}^{\alpha,\beta}(t_\alpha, t'_\beta) = -i \langle \hat{T} [\hat{\psi}_i(t_\alpha) \hat{\psi}_i^\dagger(t'_\beta)] \rangle, \tag{6}$$

where $\hat{T}$ is the chronological ordering operator along the closed time loop contour.[20] The labels α and β refer to the upper ($\alpha \equiv +$) and lower ($\alpha \equiv -$) branches on this contour. The correlation functions $\hat{G}_{ij}^{+-}$, which can be associated within this formalism with the electronic nonequilibrium distribution functions,[22] are given by the (2×2) matrix

$$\mathbf{G}_{i,j}^{+-}(t,t') = i \begin{pmatrix} \langle c_{j\uparrow}^\dagger(t') c_{i\uparrow}(t) \rangle & \langle c_{j\downarrow}(t') c_{i\uparrow}(t) \rangle \\ \langle c_{j\uparrow}^\dagger(t') c_{i\downarrow}^\dagger(t) \rangle & \langle c_{j\downarrow}(t') c_{i\downarrow}^\dagger(t) \rangle \end{pmatrix}. \tag{7}$$

Equations (2) and (3) can then be written in terms of the Fourier transform matrix elements of $\hat{G}_{ij}^{+-}(t,t')$:

$$\Delta_i = -\frac{|U_i|}{2\pi i} \int_{-\infty}^{\infty} d\omega [\mathbf{G}_{ii}^{+-}(\omega)]_{21}, \tag{8}$$

$$I_{ij} = \frac{2e}{h} \int_{-\infty}^{\infty} d\omega \left\{ t_{ij} [\mathbf{G}_{j,i}^{+-}(\omega)]_{11} - t_{ji} [\mathbf{G}_{i,j}^{+-}(\omega)]_{11} \right\}. \tag{9}$$

For the zero-voltage case the calculation of the different $\hat{G}^{+-}(\omega)$ is particularly simple because the following relation holds:

$$\hat{G}_{ij}^{+-}(\omega) = f(\omega) [\hat{G}_{ij}^a(\omega) - \hat{G}_{ij}^r(\omega)], \tag{10}$$

where $f(\omega)$ is the Fermi distribution function, and $\hat{G}^{a,r}$ are the advanced and retarded Green functions, which can be computed using recursive techniques.[23] (Note that this relation is the same as in a currentless state.)

The Green functions must be calculated self-consistently, according to Eq. (8). This is achieved starting from an initial guess for the order parameter profile and then using an iterative algorithm. As reported in Ref. 12, the electrodes can be modeled in a simple way by Bethe lattices. This choice both facilitates the computation of the Green functions and ensures a fast spatial convergence of the order parameter to its bulk values. The Bethe lattice geometry is able to simulate in a simple way the *geometrical dilution* of the current taking place when passing from a quasi-1D to a 3D structure. We have fixed the Bethe lattice coordination number $z+1 = 4$, which leads to a convergence of the order parameter within three or four layers.

IV. TRANSITION FROM POINT CONTACT TO 1D FLOW

It is interesting to analyze in detail the maximum dc Josephson current I_c that can be sustained by a SWL

with a single conducting channel as a function of its length and transmission coefficient α. Within our tight-binding model, α is a known function of the hopping parameters t_{ij}. For the results presented in this work α is varied by changing uniformly t_{ij} inside the constriction, while keeping them fixed inside the reservoirs.

For any value of α, the point-contact limit ($L_c/\xi_0 \to 0$) is well understood.[6,12,24] In this case, the phase profile can be well approximated by a step function and the current-phase relationship can be obtained analytically for a symmetric junction (details of this derivation within our formalism are given in Appendix A):

$$I(\phi) = \frac{e\alpha}{2\hbar}\frac{|\Delta(T)|^2}{|\epsilon(\phi)|}\sin(\phi)\tanh\left[\frac{|\epsilon(\phi)|}{2k_BT}\right], \qquad (11)$$

where $\epsilon(\phi) = \pm|\Delta(T)|\sqrt{1-\alpha\sin^2(\phi/2)}$ denotes the position of bound states within the superconducting gap. These bound states give the main contribution to the supercurrent across the interface. As we shall see the existence of bound states inside the gap remains even for a SWL of length much larger than ξ_0. It should be mentioned that an expression essentially equivalent to Eq. (11) was first derived by Kulik and Omel'yanchuk within a semiclassical approximation to the Bogoliubov–de Gennes equations.[25]

The maximum supercurrent in this point-contact limit can be obtained as a function of α from Eq. (11). At zero temperature we find

$$I_{c,0}(\alpha) = \frac{e\Delta}{\hbar}(1-\sqrt{1-\alpha}) \; . \qquad (12)$$

Therefore the maximum possible current through a single quantum channel is $e\Delta/\hbar$ whereas in the tunnel regime $I_{c,0} \simeq e\Delta\alpha/2\hbar$, which corresponds to the well-known Ambegaokar-Baratoff value,[26] $\pi\Delta/2eR_N$, for the single-channel case. The function $I_{c,0}(\alpha)$ is plotted in Fig. 2. Let us mention that the divergence in the derivative $\partial I_{c,0}/\partial\alpha$ as α tends to 1 is a zero-temperature feature, which is quickly smoothed at finite temperatures; at $T = 0.2T_c$, $I_{c,0}(\alpha = 1)$ is reduced by a factor of $\sim 20\%$. This suggests that the experimental observation of the quantized critical current $e\Delta/\hbar$ requires quite delicate conditions (i.e., perfect transmission, symmetric junction, very low temperatures, etc.).

At zero temperature, when L_c is increased keeping the value of α fixed, the maximum current can either decrease or increase from the $L_c = 0$ value. In Fig. 3 we represent the behavior of $I(\phi)$ with increasing L_c for three values of the transmission α. Only the positive part of $I(\phi)$ is plotted. A general trend is the appearance of multivaluation for $L_c/\xi_0 > 1$, although the precise value for this threshold ratio is dependent on α, as can be observed in Fig. 3. Note that the form of the $I(\phi)$ curves itself is strongly dependent on α; therefore there is not a simple scaling between the different set of curves. For instance, the low transmission case [Fig. 3(c)] becomes markedly different from the other two when L_c/ξ_0 increases [note the peculiar form of the 48-site case in which there appears a

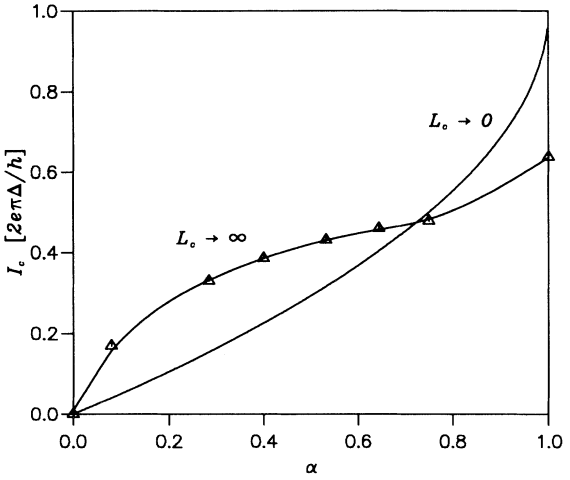

FIG. 2. Maximum supercurrent for a single-channel weak link at zero temperature in the point-contact limit ($L_c = 0$) and in the asymptotic infinite-length limit, as a function of the transmission coefficient.

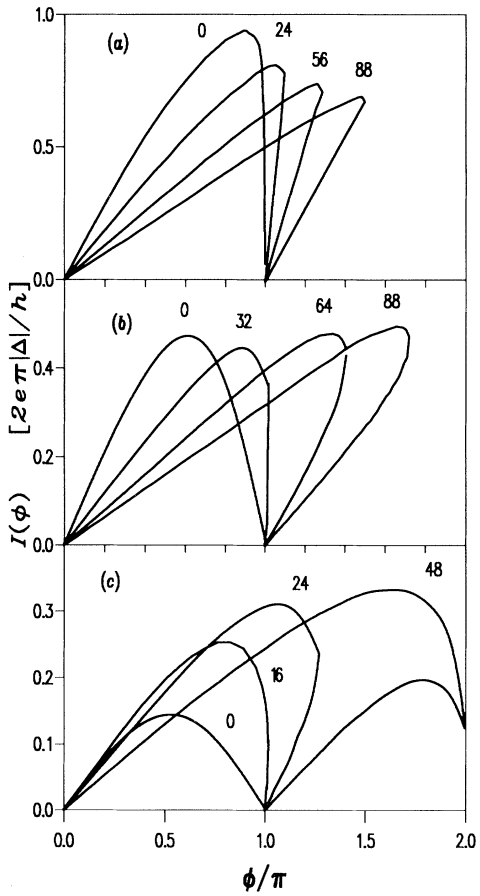

FIG. 3. Supercurrent-phase characteristics at zero temperature for different constriction lengths and three pairs of values for the transmission and the coherence length: (a) $\alpha = 1$ and $\xi_0 = 22.05$, (b) $\alpha = 0.75$ and $\xi_0 = 12.73$, and (c) $\alpha = 0.28$ and $\xi_0 = 6.37$. The coherence length and the L_c values given in the figure are measured in units of the site spacing.

cusp at $\phi = 2\pi$; for larger lengths this cusp progressively bends down while $I(\phi = 2\pi)$ tends to zero]. In the limit $L_c/\xi_0 \to \infty$, the behavior would be that of a double tunnel junctions with a $I(\phi) \sim \sin(\phi/2)$ characteristic for the upper branch.[12]

The maximum current I_c is represented in Fig. 4 as a function of L_c/ξ_0 for the three cases shown in Fig. 3 . It can be observed that when $L_c/\xi_0 \gg 1$ and for high transmission I_c decreases asymptotically to a limiting value, whereas for low transmission the trend is the opposite. On the other hand, when $L_c/\xi_0 \sim 1$ interference effects can lead to a nonmonotonic behavior of I_c with length. See for instance the intermediate transmission case ($\alpha = 0.75$) where a dip at $L_c \sim \xi_0$ is found.

The limiting case $L_c/\xi_0 \to \infty$ corresponds to a homogeneous flow in a one-dimensional superconductor in which the coupling to the left and right electrodes acts as boundary conditions. The asymptotic value of the maximum current $I_{c,\infty}$ depends on this coupling and is therefore a function of α. These values are represented by the triangles in Fig. 2, where they can be compared with the $L_c = 0$ case. It is worth noticing that for perfect transmission $I_{c,\infty}$ coincides with the depairing current of a one-dimensional superconductor, i.e., $2e\Delta/\pi\hbar$.[27] The derivation of this result within our model is given in Appendix B. The self-consistent phase gradient along the linear chain is equal to $2\Delta/\hbar v_F$ when this limit is reached.

On the other hand, for low transmission, when the matching to the electrodes is poor, the self-consistent phase drop concentrates mainly on the contacts and, as mentioned above, the system becomes equivalent to a double tunnel junction. In these conditions the maximum current is controlled basically by the transmission through a single junction. For a symmetric weak link this single-junction transmission α_1 is related to the total transmission α by $\alpha_1 \approx 2\sqrt{\alpha}$ (this relation holds only for $\alpha \ll 1$). Then, according to Eq. (11), $I_{c,\infty}(\alpha) \approx \frac{e\Delta}{\hbar}\sqrt{\alpha}$, which is qualitatively in agreement with the numerical results for small α in Fig. 2.

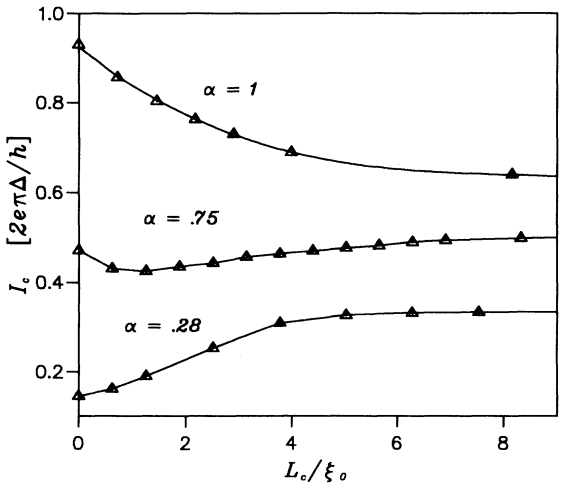

FIG. 4. Maximum supercurrent at zero temperature for the same three cases as in Fig. 3 as a function of L_c/ξ_0.

A deeper insight into the transition from the point contact to the infinite 1D case can be obtained by analyzing the evolution of the local quasiparticle spectral density $\rho_i(\omega)$ and the associated current density $j_i(\omega)$, given by

$$\rho_i(\omega) = \frac{1}{\pi}\mathrm{Im}[\hat{G}^a_{ii}(\omega)]_{11} , \tag{13}$$

$$j_i(\omega) = \frac{2e}{\hbar}\left\{t_{i,i+1}[\mathbf{G}^{+-}_{i+1,i}(\omega)]_{11} - t_{i+1,i}[\mathbf{G}^{+-}_{i,i+1}(\omega)]_{11}\right\} , \tag{14}$$

where site i is chosen to be located at the center of the constriction, where the effect of the 3D reservoirs is less pronounced. In the following discussion only energies $\omega \leq 0$ are considered as $\rho_i(\omega) = \rho_i(-\omega)$ due to $e - h$ symmetry.

For $L_c/\xi_0 \ll 1$ the most relevant feature is the appearance of a bound state in the spectra inside the gap. The position and weight of this state are a function of the phase difference ϕ and the transmission coefficient α, as noted in the discussion of Eq. (11). In this regime this state gives the main contribution to the current in the constriction: $j_i(\omega)$ is essentially a δ function at the bound state energy. In Fig. 5 the evolution of $\rho_i(\omega)$ and $j_i(\omega)$ as L_c/ξ_0 increases is represented for the case of perfect transmission. In all the cases plotted in this figure the current is the maximum one for the corresponding constriction length.

Two main features are observable in these curves: First, with increasing L_c new bound states appear in the gap. The new states initially split from the continuum, moving to energies closer to $\mu = 0$. Eventually, for $L_c \to \infty$ these states would fill the gap as shown in the uppermost curves of Fig. 5, which correspond to the uniform infinite 1D superconductor carrying the critical current (see Appendix B). The number of bound states increases very slowly with L_c/ξ_0. For instance, for L_c/ξ_0 as large as 10, only three bound states are present.

On the other hand, the current density of the continuous part of the spectrum ($\omega \leq -\Delta$), which at $L_c/\xi_0 \to 0$ is negligible, becomes more important with increasing length, and in the limit $L_c/\xi_0 \to \infty$ gives a contribution which has the opposite sign to the total current.[28]

To conclude this section, let us analyze briefly the nature of the bound states. The study of their spatial distribution shows that they correspond to Cooper pairs that are extended along the constriction region and decay exponentially inside the reservoirs within a typical length $\sim \xi_0$. In Fig. 6 we represent the local spectral weight of the bound states along the constriction. It corresponds to case (d) in Fig. 5, in which three bound states are present. As can be seen in Fig. 6, the bound state closer to $\omega = 0$ has always a nodeless form, while the number of oscillations increases for the bound states with a larger binding energy. This situation is reminiscent of the one found for a potential well; however, one should keep in mind that the bound states in the present case are due to variations of the superconducting phase on a finite spatial region (the constriction region), disappearing when

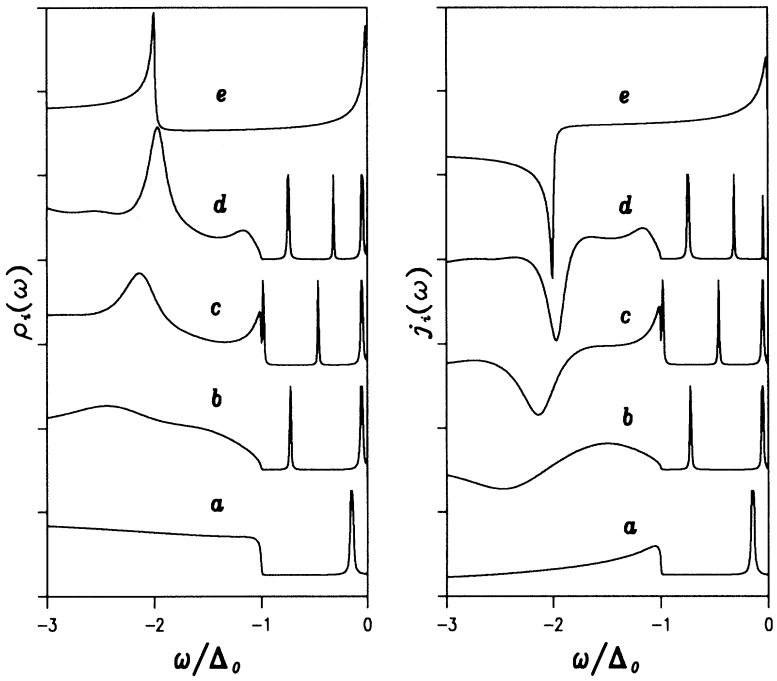

FIG. 5. Local spectral and supercurrent density at the center of the constriction for the $\alpha = 1$ case and different values of L_c/ξ_0: (a) $L_c/\xi_0 = 2.18$, (b) $L_c/\xi_0 = 5.80$, (c) $L_c/\xi_0 = 9.43$, (d) $L_c/\xi_0 = 13.06$, and (e) $L_c/\xi_0 = \infty$. The curves are displaced upwards with respect to case (a) for clarity. All cases correspond to the maximum supercurrent.

the total phase drop is zero. In junctions of the type S-S'-S or S-N-S with large variations in the pairing potential one could find bound states even without current.[5,17,29] We should comment that the spatial distribution of the current carried by a bound state follows closely that of its weight. Actually, we have verified that the ratio between current and weight for each bound state is practically a constant along the constriction region. This result further illustrates the fact that the bound states correspond to Cooper pairs with a well-defined velocity inside the constriction.

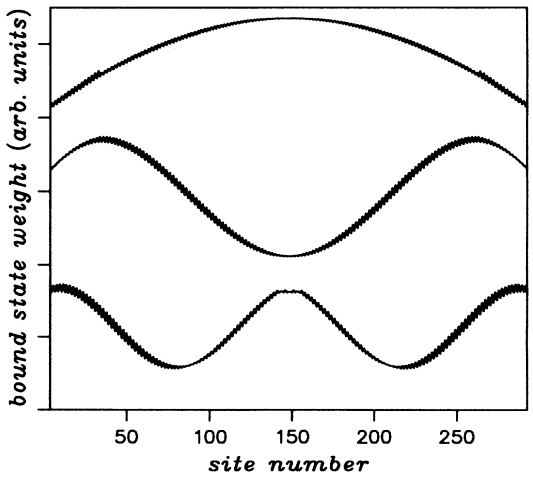

FIG. 6. Spectral weight along the constriction for the bound states appearing in case (d) of Fig. 5. The order from top to bottom corresponds to increasing binding energy.

V. SELF-CONSISTENT ORDER-PARAMETER PROFILES AT ZERO TEMPERATURE

The self-consistent determination of the order-parameter profiles is essential for a weak link of length $L_c \geq \xi_0$, whereas for $L_c \ll \xi_0$, the point-contact limit, the detailed form of the self-consistent profiles becomes irrelevant. In this latter case the current-phase relationship is given to a high degree of accuracy by Eq. (11).[6,12]

In this section we present results for $L_c \geq \xi_0$ in order to illustrate the effects of self-consistency. Although some of the overall features appearing in the profiles can be expected on intuitive physical grounds, their detailed form reflects a complex interplay between the different model parameters.

In Fig. 7 we represent the phase and modulus profiles for fixed L_c and ϕ, and three different values of the transmission coefficient. All three results correspond to the upper branch of the $I(\phi)$ characteristic.

The common general features of the profiles along the upper branch are displayed in Fig. 7. They consist of a constant phase gradient along the constriction together with localized drops at the contacts with the reservoirs. One could draw an analogy between these localized phase drops and the voltage drops at the contacts with the leads in a normal mesoscopic sample (Sharvin resistance).[8,30] On the other hand, the modulus is on average constant along the constriction.

Superimposed to this general structure, oscillations with a spatial period $\lambda_F/2$ can be observed.[12] These oscillations have a maximum amplitude in the proximity of the contacts and decay when moving inside the constriction with a typical decaying length $\sim \xi_0$. This behavior is most clearly seen in case (c) of Fig. 7, which corre-

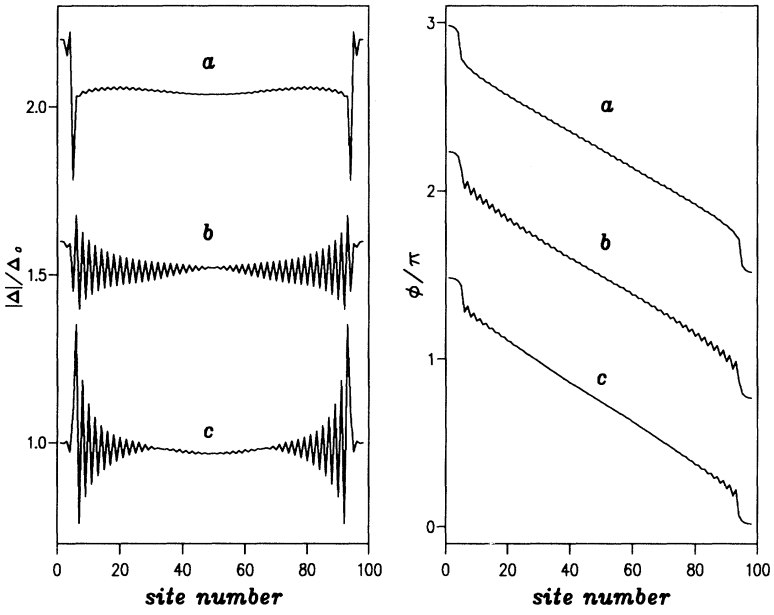

FIG. 7. Upper branch self-consistent order-parameter profiles (phase and modulus) for a total phase drop $\phi = 4.60$ and fixed constriction length $L_c = 88$. The transmission and coherence length correspond to the three cases shown in Fig. 3. The curves (a) and (b) are displaced upwards with respect to case (c).

sponds to $L_c/\xi_0 \gg 1$ and low transmission, leading to oscillations which are more concentrated near the contacts, having a larger amplitude due to the presence of larger barriers. This interference phenomenon is a consequence of the phase coherence of normal electrons along the mesoscopic system. As shown in the next section, there is a gradual disappearance of the oscillations with increasing temperature. Let us remark that a similar oscillation pattern can be found for the electrostatic potential along a normal mesoscopic constriction.[30–32]

When $I(\phi)$ is a multivalued function, the solutions in the lower branch exhibit a very different character: They correspond to the solitonic solutions predicted by GL theory.[13,19,33] In Fig. 8 we show the phase and modulus profiles for this second type of solution, corresponding to three different values of L_c with fixed α and ϕ. We have chosen $\phi \sim \pi$ where the specific features of these solutions are more pronounced. It can be observed that the gross features are the ones predicted by GL theory, namely, an abrupt phase drop together with a significant depression of the modulus which nearly goes to zero at the center of the constriction. Note that this profile leads to a very low value of the current. In addition to this general shape, an oscillation pattern of period $\lambda_F/2$ is again found. An interesting feature is the existence of a well-defined core region of length $\sim \xi_0$ where the phase drop takes place

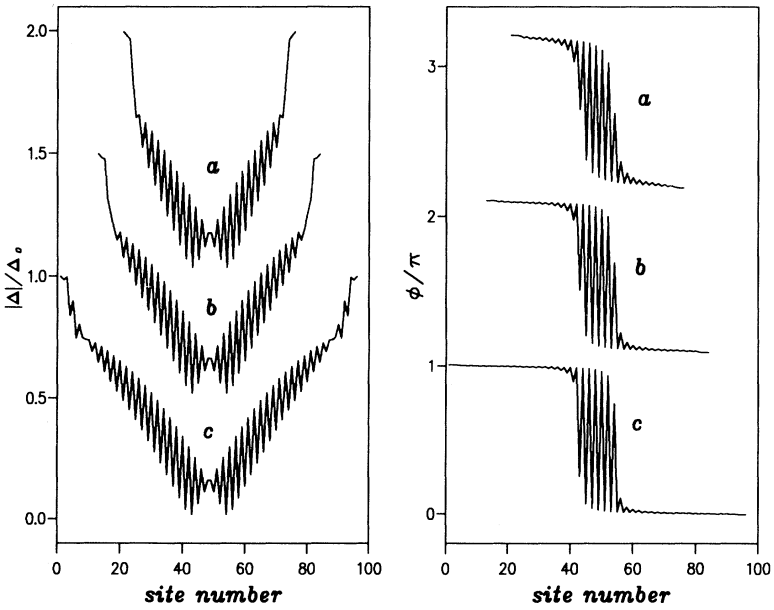

FIG. 8. Lower branch self-consistent order-parameter profiles (phase and modulus) for a total phase drop $\phi = 3.20$, $\alpha = 0.75$, and $\xi_0 = 12.73$ and three values of the constriction length: (a) $L_c = 48$, (b) $L_c = 64$, and (c) $L_c = 88$.

and the modulus is nearly zero (see Fig. 8). This core remains practically unchanged with increasing L_c. This is a feature that cannot be predicted by GL theory, the reason being, as we shall see in the next section, that the core size vanishes when T approaches T_c.

The question about the stability of these type of solution deserves some attention. As discussed by Langer and Ambegaokar,[33] these solutions correspond for a homogeneous infinite system to saddle points of the free energy. However, for a finite weak link these solutions are presumably unstable.[13] As a matter of fact, we have verified that these solutions cannot be reached using a simple iterative algorithm no matter how close from the actual solution one starts. Instead, the use of a more sophisticated algorithm (Broyden type[34]) capable of obtaining any sort of extrema leads to the solitonic solution without difficulties.

VI. EFFECTS OF FINITE TEMPERATURE

In this section we discuss the effects of a finite temperature on the $I(\phi)$ characteristic and on the self-consistent profiles for our model weak link. Although $L_c/\xi_0(T)$ is the main parameter controlling the different regimes (point contact, infinite homogeneous superconductor), there is not a simple scaling of the system properties as a function of this single parameter.

This becomes apparent when studying the evolution of the different properties with temperature. Figure 9 shows the current-phase relationship for the same set of parameters as in Fig. 3(b) and three increasing values of temperature: $0.3T_c$, $0.5T_c$, and $0.95T_c$. As one can observe, the phase interval where $I(\phi)$ is multivalued gradually disappears while $I(\phi)$ tends to the familiar $\sin\phi$ dependence as $T \to T_c$. This behavior can be qualitatively understood noticing that for a given length and T sufficiently high ($T \to T_c$), the condition $L_c/\xi_0(T) \ll 1$ is fulfilled, and the system should behave like a point contact, in which case Eq. (11) approximately holds. Note, however, in Fig. 9(c), that a significant deviation from the maximum current value predicted by Eq. (11), i.e., $I_c = \frac{\pi}{2eR_N}\frac{\Delta^2(T)}{K_BT}$, is observed as soon L_c is a small fraction of $\xi_0(T)$. This is due to the fact that the self-consistent phase profile, even for small $L_c/\xi_0(T)$, deviates from a step function form.

The possible scaling of the maximum supercurrent with $L_c/\xi_0(T)$ can be analyzed with the help of Fig. 10. For these values of the transmission coefficient ($\alpha \sim 0.75$), a universal behavior of the type $\sim \exp[-AL_c/\xi_0(T)]$ is only observed for temperatures larger than $0.5T_c$. For lower transmission this departure from a universal behavior is even more pronounced; the maximum supercurrent at low temperatures is in this case an increasing function of $L_c/\xi_0(T)$ (see bottom curve in Fig. 4) while the $\exp[-AL_c/\xi_0(T)]$ behavior is only recovered for $T \to T_c$.

Let us briefly comment on the effects of finite temperature on the self-consistent order-parameter profiles. Either in the upper and lower branch solutions there is a

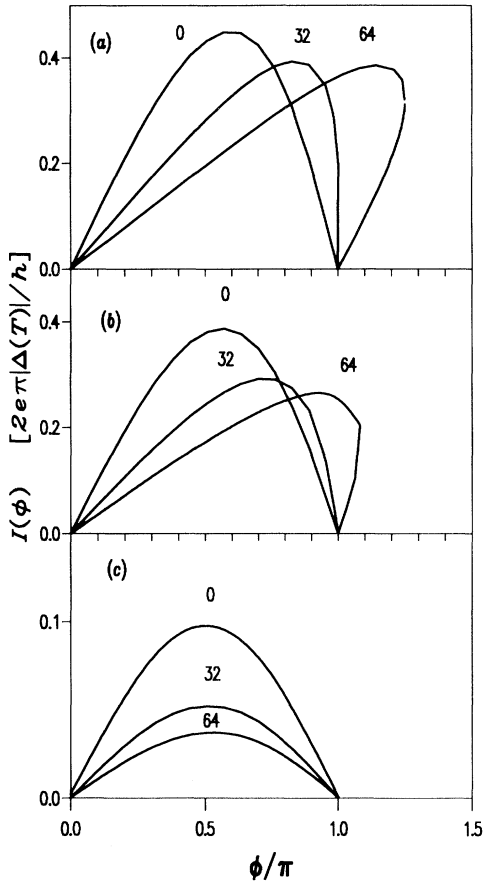

FIG. 9. Supercurrent-phase characteristics for $\alpha = 0.75$, different constriction lengths and three values of temperature: (a) $T = 0.3T_c$ and $\xi_0(T) = 12.78$, (b) $T = 0.5T_c$ and $\xi_0(T) = 13.37$, and (c) $T = 0.95T_c$ and $\xi_0(T) = 39.79$.

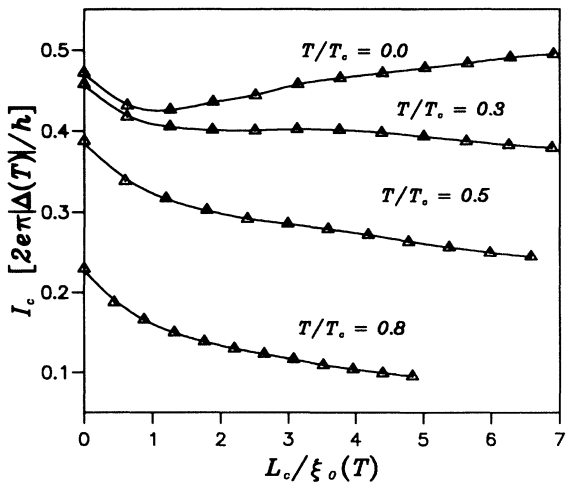

FIG. 10. Maximum supercurrent for $\alpha = 0.75$ as a function of $L_c/\xi_0(T)$ for increasing values of temperature.

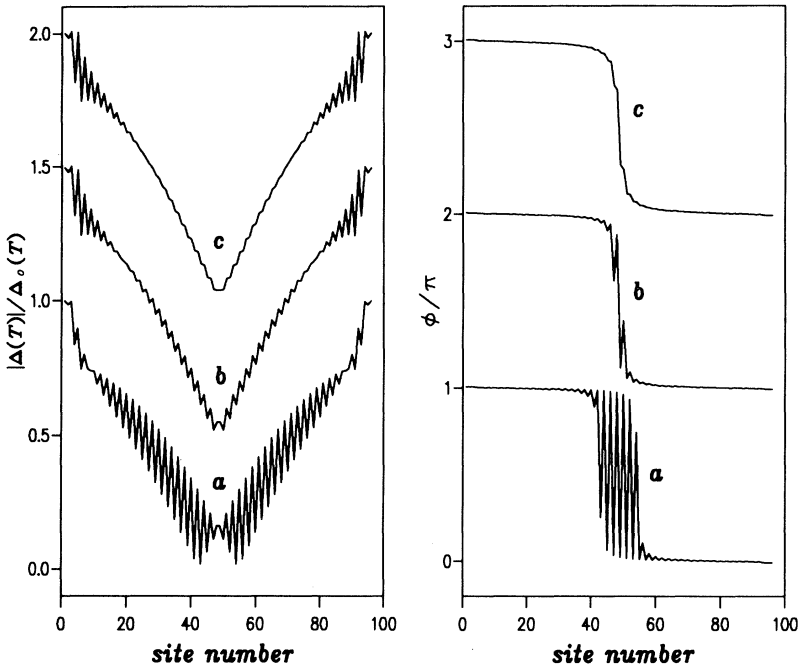

FIG. 11. Lower branch self-consistent order-parameter profiles (phase and modulus) for a total phase drop $\phi = 3.20$, $\alpha = 0.75$, and $L_c = 88$ and three values of temperature: (a) $T = 0$, (b) $T = 0.3T_c$, and (c) $T = 0.5T_c$.

gradual disappearance of the $\lambda_F/2$ oscillations (see Fig. 11). In the upper branch solutions there are no notable changes in the phase profiles, besides the smoothing of the oscillations pattern, the expected Josephson current decrease being due to the global lowering of $\Delta(T)$ in the whole system. The evolution of the solitonic profiles with temperature is more unusual. This is illustrated in Fig. 11, where it can be observed how the solitonic core, which at zero temperature has a size $\xi_0(0)$, shrinks and eventually disappears as temperature increases. This evolution is particularly clear in the phase profiles of Fig. 11.

VII. CONCLUDING REMARKS

We have presented a self-consistent solution of the microscopic Bogoliubov–de Gennes equations for a mesoscopic SWL. As illustrated in the present work, our method allows us to analyze situations where spatial variations of the superconducting order parameter over length scales smaller or comparable to the coherence length are important, and its self-consistent determination becomes necessary. As discussed in this work, the usual GL approach may not be valid for a mesoscopic sample at low temperatures. Our results reveal that for low temperatures and due to coherence effects, there is no universal behavior of the SWL properties as a function of $L_c/\xi_0(T)$. These coherence effects are also reflected in the self-consistent order-parameter profiles, which exhibit features that cannot be predicted by GL theory.

We have analyzed in detail the transition from the point-contact limit to the infinite 1D superconductor characterized by a continuous spectrum. The appearance of bound states seems to be a general feature of a weak link of mesoscopic size due to the spatial inhomogeneity of the pairing potential in the constriction region. Even in the absence of a well-defined pairing potential well, spatial variations of the superconducting phase associated with a supercurrent can lead to the formation of bound states.

The application of the present approach to the description of submicrometer superconducting devices of current experimental interest,[1] which may include S-N or S-Sm interfaces and where the sample geometry plays an important role, is under progress in our laboratory.

ACKNOWLEDGMENTS

Support by Spanish CICYT (Contract No. PB89-0165) is acknowledged. The authors are indebted to F. Flores, J. C. Cuevas, and F. Sols for useful discussions. One of us (A.L.Y.) acknowledges support by the European Community under Contract No.CI1*CT93-0247.

APPENDIX A

In this appendix we give a short account of the derivation of the supercurrent-phase relationship for a SWL in the point-contact limit. Starting from Eq. (9), the current evaluated at the interface between the electrodes can be written as

$$I = \frac{2e}{h}\int_{-\infty}^{\infty} d\omega f(\omega)\,\mathrm{Tr}[\mathbf{T}_{LR}(\mathbf{G}^a_{RL} - \mathbf{G}^r_{RL}) - \mathbf{T}_{RL}(\mathbf{G}^a_{LR} - \mathbf{G}^r_{LR})]_{11}\,, \tag{A1}$$

where L and R indicate the left and right electrodes and Tr denotes trace over orbitals at the interface. The hopping elements in the superconducting broken-symmetry representation are given by the 2×2 matrix $\mathbf{T}_{i,j}=\tau_3 t_{i,j}$, where τ_3 is a Pauli matrix and i,j denote any pair of orbitals.

The Green functions appearing in this expression can be obtained from the ones corresponding to the uncoupled electrodes ($\mathbf{T}_{LR}=0$) $\mathbf{g}_L^{a,r}$, $\mathbf{g}_R^{a,r}$, using Dyson equations:

$$\mathbf{G}_{LR}^{a}=\mathbf{g}_L^{a}\mathbf{T}_{LR}\mathbf{g}_R^{a}\mathbf{D}_{LR}^{a}\ , \tag{A2}$$

where $\mathbf{D}_{LR}^{a}=[\mathbf{I}-\mathbf{T}_{LR}\mathbf{g}_R^{a}\mathbf{T}_{RL}\mathbf{g}_L^{a}]^{-1}$ with similar expressions for the retarded quantities. Substituting in Eq. (A1) and performing some elementary algebra, we obtain

$$I=\frac{2e}{h}\int_{-\infty}^{\infty}d\omega f(\omega)\,\mathrm{Tr}[(\mathbf{D}_{RL}^{a}-\mathbf{D}_{LR}^{a}) -(\mathbf{D}_{RL}^{r}-\mathbf{D}_{LR}^{r})]_{11}\ . \tag{A3}$$

This equation is valid for a general junction geometry with any number of conducting channels. For the simple case of a symmetric junction with a single channel, an analytical expression can be derived for $I(\phi)$ if a steplike phase-profile is assumed:

$$I=\frac{4ei}{h}|t_{LR}|^2\sin\phi\int_{-\infty}^{\infty}d\omega f(\omega)\left[\frac{\tilde{g}_{L,21}^{a}(\omega)\tilde{g}_{R,12}^{a}(\omega)}{\det[D_{LR}^{a}(\omega)]} -\frac{\tilde{g}_{L,21}^{r}(\omega)\tilde{g}_{R,12}^{r}(\omega)}{\det[D_{LR}^{r}(\omega)]}\right]\ , \tag{A4}$$

where the tilde indicates that the phase factor has been removed, i.e., $\tilde{g}_{L,21}=e^{-i\phi_L}g_{L,21}$ and $\tilde{g}_{R,12}=e^{i\phi_R}g_{R,12}$. The integration in Eq. (A4) can be performed analytically as a contour integration by realizing that the main contribution (up to corrections of the order Δ/ϵ_F) is given by the zeros within the superconducting gap of $\det[D_{LR}^{a}(\omega)]$, which correspond to the bound states commented in Sec. IV. The contribution from these poles yields Eq. (11) straightforwardly.

APPENDIX B

A simple derivation of the depairing current for a 1D superconductor within our tight-binding model is given below.

The Hamiltonian in this case is the one given in Eq. (1) with $t_{ij}=t(\delta_{i,j+1}+\delta_{i,j-1})$, $\epsilon_i=0$, and $\Delta_j=\Delta_q e^{iqj}$. This last relation holds for a uniform superconducting flow, with Cooper pairs of net momentum q.[17] For an infinite system, the Green functions adopt a simpler form in the k representation:

$$[\mathbf{G}_{k,q}(\omega)]_{11}=\frac{\omega+\epsilon_{-k+q}}{(\omega-\epsilon_k)(\omega+\epsilon_{-k+q})-\Delta_q^2}\ , \tag{B1}$$

$$[\mathbf{G}_{k,q}(\omega)]_{12}=-\frac{\Delta_q}{(\omega-\epsilon_k)(\omega+\epsilon_{-k+q})-\Delta_q^2}\ , \tag{B2}$$

where $\epsilon_k=2t\cos k-\mu$. The poles of these functions at $E_{k,q}^{\pm}=\delta\epsilon_{k,q}\pm\sqrt{\bar{\epsilon}_{k,q}^2+\Delta_q^2}$, where $\delta\epsilon_{k,q}=(\epsilon_k-\epsilon_{-k+q})/2$ and $\bar{\epsilon}_{k,q}=(\epsilon_k+\epsilon_{-k+q})/2$, give the excitation spectrum of a current carrying 1D superconductor. The critical momentum q_c, which corresponds to the condition that the gap in the excitation spectrum goes to zero, is given, for sufficiently small q_c ($q_c\sin k_F\ll1$), by $q_c=\Delta_0/t\sin k_F$.

It can be shown that the self-consistent order parameter Δ_q for $q\le q_c$ is in this limit equal to Δ_0 up to corrections of order q^2. Actually, these corrections are positive, leading to a small increase in Δ_q with increasing current.

The local spectral density $\rho(\omega)$ and the local current density $j(\omega)$ discussed in Sec. IV can be directly calculated from $\mathbf{G}_{k,q}(\omega)$. In particular, the total current is given by

$$I=\frac{4e}{\pi\hbar}t\int_{-\pi}^{\pi}dk\sin k\int_{-\infty}^{\infty}d\omega f(\omega)\mathrm{Im}\left[\mathbf{G}_{k,q}^{a}(\omega)\right]_{11}\ . \tag{B3}$$

At zero temperature, the integral over ω can be easily performed, giving

$$I=\frac{et}{\pi\hbar}\int_{-\pi}^{\pi}dk\frac{\bar{\epsilon}_{k,q}\sin k}{\sqrt{\bar{\epsilon}_{k,q}^2+\Delta_q^2}}\simeq\frac{2e}{\pi\hbar}t\sin k_F\ q\ , \tag{B4}$$

where the last approximation holds in the limit $q\sin k_F\ll1$. Thus, for $q=q_c$ the depairing current is simply $\frac{2}{\pi}e\Delta/\hbar$, in agreement with Ref. 27.

[1] A. Kastalsky, A. W. Kleinsasser, L. H. Greene, R. Bhat, F. P. Milliken, and J. P. Harvison, Phys. Rev. Lett. **67**, 3026 (1991); C. Nguyen, H. Kroemer, and E. L. Hu, *ibid.* **69**, 2847 (1992); U. T. Petrashov, V. N. Antonov, P. Delsing, and T. Claeson, *ibid.* **70**, 347 (1993); P. Xiong, G. Xiao, and R. B. Laibowitz, *ibid.* **71**, 1907 (1993).

[2] C. W. J. Beenakker, Phys. Rev. B **46**, 12841 (1992).

[3] C. J. Lambert, V. C. Hui, and S. J. Robinson, J. Phys. Condens. Matter **5**, 4187 (1993).

[4] P. F. Bagwell, Phys. Rev. B **46**, 12573 (1992).

[5] U. Gunsenheimer, U. Schussler, and R. Kummel, Phys. Rev. B **49**, 6111 (1994).

[6] A. Furusaki, H. Takayanagi, and M. Tsukada, Phys. Rev. Lett. **67**, 132 (1991); C. W. J. Beenakker and H. van Houten, Phys. Rev. Lett. **66**, 3056 (1991); C. W. J. Beenakker, in *Proceedings of the 14th Taniguchi International Symposium on Transport Phenomena in Mesoscopic Systems*, edited by H. Fukuyama and T. Ando (Springer, Berlin, 1992).

[7] R. Landauer, Philos. Mag. **21**, 863 (1970).

[8] M. Buttiker, Y. Imry, R. Landauer, and S. Pinhaes, Phys. Rev. **31**, 6207 (1985); M. Buttiker, Phys. Rev. Lett. **57**, 1761 (1986).

[9] A. D. Stone, Phys. Rev. Lett. **54**, 2692 (1985); J. Ferrer,

A. Martín-Rodero, and F. Flores, Phys. Rev. B **38**, 10 113 (1988); J. Masek and B. Kramer, Z. Phys. B **75**, 57 (1989); A. Levy Yeyati, J. Phys. Condens. Matter **2**, 6533 (1990).
[10] G. E. Blonder, M. Tinkham, and T. M. Klapwijk, Phys. Rev. B **25**, 4515 (1982).
[11] N. Agrait, J. G. Rodrigo, C. Sirvent, and S. Vieira, Phys. Rev. B **48**, 8499 (1993).
[12] A. Martín-Rodero, F. J. García-Vidal, and A. Levy Yeyati, Phys. Rev. Lett. **72**, 554 (1994).
[13] K. K. Likharev, Rev. Mod. Phys. **51**, 101 (1979).
[14] L. G. Aslamazov and A. I. Larkin, Pis'ma Zh. Eksp. Teor. Fiz. **9**, 150 [JETP Lett. **9**, 87 (1969)].
[15] GL theory is derived from the microscopic Bogoliubov – de Gennes equations assuming that spatial variations in $\Delta(T)$ take place on length scales much larger than ξ_0. See L. P. Gor'kov, Zh. Eksp. Teor. Fiz. **36**, 1918 (1959) [Sov. Phys. JETP **9**, 1364 (1960)]. This condition may not be fulfilled for a typical mesoscopic sample where geometrical boundaries introduce strong variations on $\Delta(T)$ on length scales of the order or smaller than ξ_0.
[16] One should mention that there has been a large number of works (especially during the 1970s) devoted to the study of SWL's and based on simplified semiclassical versions of the complete Bogoliubov – de Gennes equations. For a review on these works see Ref. 13.
[17] P. G. de Gennes, *Superconductivity of Metals and Alloys* (Benjamin, New York, 1966).
[18] A. Furusaki and M. Tsukada, Solid State Commun. **78**, 299 (1991).
[19] F. Sols and J. Ferrer, Phys. Rev. B **49**, 15913 (1994).
[20] L. V. Keldysh, Sov. Phys. JETP **20**, 1018 (1965).
[21] Y. Nambu, Phys. Rev. **117**, 648 (1960).
[22] L. P. Kadanoff and G. Baym, *Quantum Statistical Mechanics* (Benjamin, New York, 1962).
[23] See, for instance, A. Levy Yeyati, Phys. Rev. B **45**, 14189 (1992).
[24] G. B. Arnold, J. Low Temp. Phys. **59**, 143 (1985).
[25] O. Kulik and A. N. Omel'yanchuk, Fiz. Nizk. Temp. **3**, 945 (1977); **4**, 296 (1978) [Sov. J. Low Temp. Phys. **3**, 459 (1977); **4**, 142 (1978)].
[26] V. Ambegaokar and A. Baratoff, Phys. Rev. Lett. **10**, 486 (1963); **11**, 104 (1963).
[27] P. F. Bagwell, Phys. Rev. B **49**, 6841 (1994).
[28] The relative contribution to the supercurrent coming from bound and scattering states has been discussed in Refs. 4 and 5 for the case of S-N-S junctions.
[29] M. J. DeWeert and G. B. Arnold, Phys. Rev. Lett. **55**, 1522 (1985); Phys. Rev. B **39**, 11307 (1989).
[30] P. L. Pernas, A. Martín-Rodero, and F. Flores, Phys. Rev. B **41**, 8553 (1990).
[31] M. Buttiker, Phys. Rev. B **40**, 3409 (1989).
[32] J. L. D' Amato and H. Pastawski, Phys. Rev. B **41**, 7411 (1990).
[33] J. S. Langer and V. Ambegaokar, Phys. Rev. **164**, 498 (1967).
[34] D. Vanderbilt and S. G. Louie, Phys. Rev. B **30**, 6118 (1984).